Journal of Alloys and Compounds 842 (2020) 155120

Contents lists available at ScienceDirect

Journal of Alloys and Compounds

journal homepage: http://www.elsevier.com/locate/jalcom

Studies of structural, magnetic and dielectric properties of X-type Barium Zinc hexaferrite $Ba_2Zn_2Fe_{28}O_{46}$ powder prepared by combustion treatment method using *ginger* root extract as a green reducing agent

Amrin R. Kagdi [a], Robert C. Pullar [b], Sher Singh Meena [c], Rajshree B. Jotania [a, *], Khalid Mujasam Batoo [d]

[a] Department of Physics, Electronics and Space Science, University School of Sciences, Gujarat University, Ahmedabad, 380 009, Gujarat, India
[b] Department of Engineering of Materials and Ceramics/CICECO - Aveiro Institute of Materials, University of Aveiro, Aveiro, 3810-193, Portugal
[c] Solid State Physics Division, Bhabha Atomic Research Centre, Mumbai, 400 085, India
[d] King Abdullah Institute for Nanotechnology, King Saud University, Riyadh, 11451, Saudi Arabia

ARTICLE INFO

Article history:
Received 25 December 2019
Received in revised form
24 March 2020
Accepted 8 April 2020
Available online 19 April 2020

Keywords:
Green synthesis
X-type hexaferrite
Ginger root extract
Magnetic properties
Dielectric properties

ABSTRACT

Various quantities of *ginger* (Zingiber officinale) root extract were used to prepare X-type Barium–Zinc hexaferrite with the chemical composition $Ba_2Zn_2Fe_{28}O_{46}$. The powders were prepared using a combustion treatment method, being pre-heated at 550 °C for 4 h with the *ginger* as a fuel, followed by final heating to 900 °C for 5 h and natural cooling to room temperature to obtain $Ba_2Zn_2Fe_{28}O_{46}$ hexagonal ferrite powder. The phase composition of heated powder samples was investigated by X-ray diffraction (XRD), indicating the formation of a mixture of X-type and hematite (α-Fe_2O_3). Up to 82.6%, X-ferrite was formed at 900 °C with 52.5 g of *ginger* root extract. Dielectric analysis of the prepared samples shows the frequency-dependent phenomena. All samples were hard magnets, with coercivity values (H_C) between 262.2 and 318.3 kA m^{-1}, and squareness ratios > 0.5. The sample prepared with 52.5 g *ginger* root extract possesses the highest value of saturation magnetisation ($M_S = 33.87$ Am^2 kg^{-1}) in comparison with the other prepared samples. Therefore, *ginger* was shown to be a useful natural plant extract as a reducing fuel for the low-temperature synthesis of X-ferrites. The sample prepared with 35 g ginger root extract shows a broad loss tangent resonance peak between 10 kHz and 100 kHz, while other samples show loss tangent resonance peaks between 300 kHz and 2 MHz frequency range.

1. Introduction

Currently, sustainable fresh approaches that use green chemistry to improve and protect our environment are the main concerns in many areas of research. Preparation of novel magnetic materials has become very attractive due to their potential applications in radar absorbing materials (RAM), electronics [1,2], high-density magnetic recording [3–6], biocompatible magnetic nanoparticles for cancer treatment [7–10] and magnetic resonance imaging (MRI) [11,12]. The development of biodegradable and cost-efficient synthesis methods of nanomaterial remains a scientific challenge. Nanotechnology is also important to defeat the environmental issues caused by chemical industries such as oils [13], organic dyes [14], mercury, and wastewater. Common nanoparticle synthesis using chemical methods often involves harmful chemicals and solvents which may affect the human body and environment. Hence, biological methods using natural plants or plant extracts for the preparation of nanoparticles can be used as important substitutes for chemical methods [15–18].

There are a large number of methods used for the synthesis of nanoparticles/microparticles such as co-precipitation [19], sol-gel [20,21], microemulsion [22] and standard ceramic methods [23,24], but these methods are often not environmentally friendly as reagents and solvents used in these chemical processes can be flammable or toxic. To overcome this, green synthesis of nanoparticles using eco-friendly materials like plant extracts [25], microorganisms such as fungi, yeast [26] and bacteria [27] is a low

* Corresponding author.
E-mail address: rbjotania@gmail.com (R.B. Jotania).

https://doi.org/10.1016/j.jallcom.2020.155120
0925-8388/

cost, and time reducing alternative. Different plants, roots, leaves, fruits, fruit peel, seeds, and their extracts have been used for the preparation of magnetic nanomaterials [25,28–30].

Ginger (Zingiber officinale) is a flowering plant and its root; rhizome is used as a spice [31]. An active constitute called gingerol in it is responsible for most of the health benefits from ginger [32]. *Ginger* is the world's most cultivated herb from its origin to the present having good historic and medicinal value as a digestive aid, aphrodisiac, etc., over thousands of years [33]. *Ginger* remains an important ingredient of many traditional herbal remedies, as it has a history of multiple uses [34]. Many anti-inflammatory and anti-oxidant compounds such as capsaicin, beta-carotene, pantothenic acid, curcumin, caffeic acid, and salicylate are present in it. Also, active compounds like shogaol, zerumbone, terpenoids, flavonoids, paradol, and zingerone present in ginger provide many health benefits [35].

Ginger can be used as a reducing agent for the preparation of nanomaterials as it possesses good antioxidant properties [36–38]. It has been reported that antioxidant properties are associated with the reducing power of biologically active compounds [39,40], useful during combustion synthesis.

Antioxidant activity and components vary greatly and depend on the extracting solvent and its concentration [41]. In comparison with other work, our approach is an appropriate, inexpensive, time reducing and eco-friendly route for the green synthesis of X-type barium-zinc hexaferrite. This procedure is easier compared to earlier reported, being prepared from metal nitrates in water. To the best of our knowledge, it is the first time that barium-zinc hexaferrite (along with some hematite) has been formed at 900 °C by using *ginger* root extract as a reducing agent in reactions.

In the present study, we have used different weights of *ginger* root to prepare X-type hexaferrites ($Ba_2Zn_2Fe_{28}O_{46}$) by the combustion treatment method and investigated the effect of the different amounts of ginger root on phase formation, as well as on magnetic and dielectric properties.

2. Experimental procedure

2.1. Ginger extract preparation

Fresh *ginger* root (~200 g) was taken from the market and cleaned with distilled water. The *ginger root* was first peeled before cutting and then boiled for 45 min in 200 ml distilled water to get *ginger* root extract. The resulting extract solution was filtered using a filter paper.

2.2. X-type ferrite synthesis

Stoichiometric quantities of barium nitrate $Ba(NO_3)_2$ (≥99.0% pure, Sigma–Aldrich), zinc nitrate $Zn(NO_3)_2.6H_2O$ (≥98.0% pure, Sigma–Aldrich) and ferric nitrate $Fe(NO_3)_3.9H_2O$ (≥98.0% pure, Sigma–Aldrich) were dissolved one by one in a total solution of 100 ml of *ginger* root extract. Precursor solutions were made with 0.0, 17.5, 35.0, 52.5, and 70.0 g of *ginger* root and in all cases a total of 51.79 g of metal salts were added. During this process, the solution was continuously stirred using a magnetic stirrer. The prepared mixture was heated at 90 °C in an oil bath to obtain a gel. The obtained gel was then dried in a muffle furnace at 100 °C for 20 h, to remove water. The resulting dried powder was ground in a mortar and pestle and then preheated at 550 °C for 4 h. The preheated powder was finally heated to 900 °C for 5 h, in a muffle furnace and allowed to cool naturally to room temperature to obtain the $Ba_2Zn_2Fe_{28}O_{46}$ hexaferrite powder. Fig. 1 shows the flowchart for the preparation of the X-type $Ba_2Zn_2Fe_{28}O_{46}$ hexaferrite powder. Heated samples were coded as Sample (A), Sample (B), Sample (C), Sample (D) and Sample (E) for the $Ba_2Zn_2Fe_{28}O_{46}$ hexaferrite prepared with 17.5, 35.0, 52.5, 70.0 and 0.0 g of *ginger* root extract, respectively.

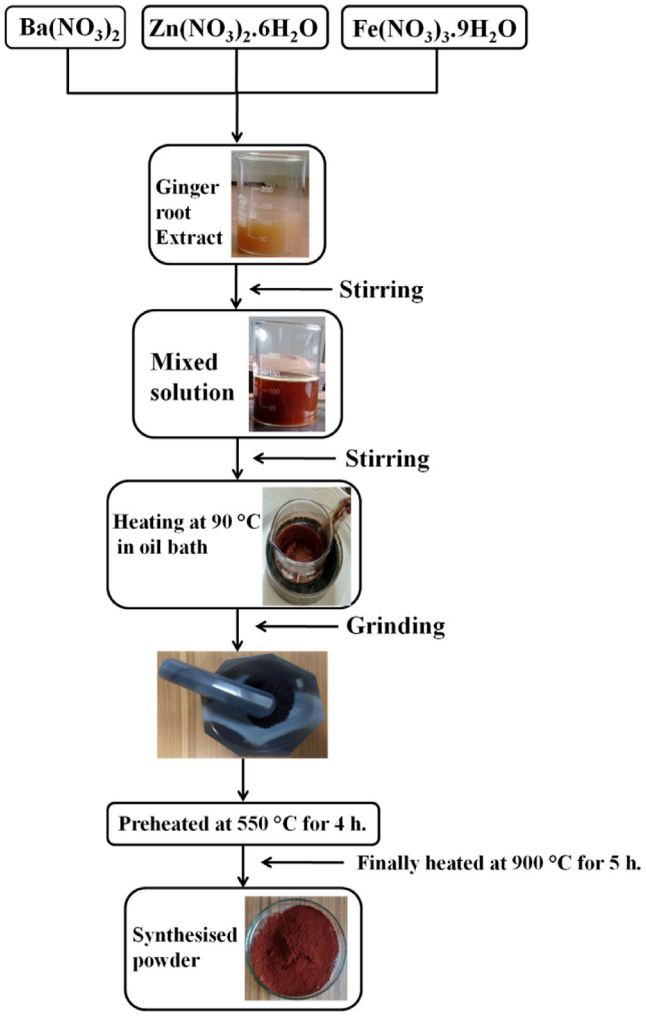

Fig. 1. Flowchart for the preparation of X-type hexaferrite $Ba_2Zn_2Fe_{28}O_{46}$ powder.

2.3. Characterisation

A FTIR spectrometer (Bruker Tensor 27 Model) was used to record infrared (IR) spectra of all heated samples over the wavenumber range of 4000–400 cm^{-1} at room temperature. KBr pellet method was used to record IR spectra. X-ray diffraction (XRD) technique was used to identify the crystalline phase formation, XRD patterns of all samples were recorded using a Rigaku X-ray diffractometer with Cu - K_α radiation ($\lambda = 1.5406$ Å), and the 2θ scanning range was 20°–80° with equal steps of 0.02°. The surface morphology of all samples was investigated using a Nano Nova 450 Field Emission Gun Scanning Electron Microscope (FEG-SEM). The magnetic hysteresis loops were recorded at room temperature under an applied magnetic field of ±1.0 T using a vibrating sample magnetometer (EG & G Princeton Applied Research instrument, Model 4500) The low-frequency dielectric measurements were carried out at room temperature over a frequency range of 100 Hz to 2 MHz using a Precision LCR meter (Agilent E4980A). The pellets of sintered ferrite powder were made using a hydraulic press for low-frequency dielectric measurements and density measurements.

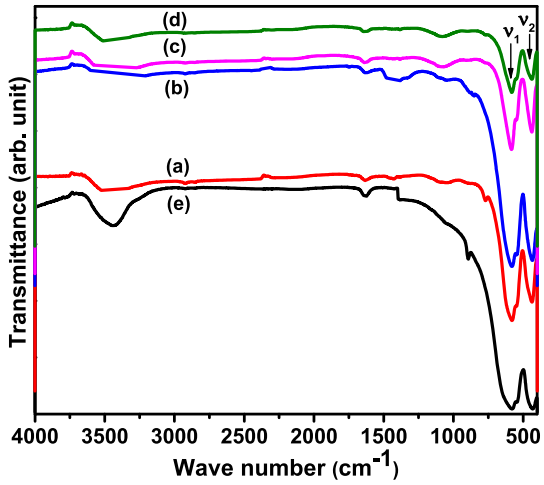

Fig. 2. FTIR spectra of X-type $Ba_2Zn_2Fe_{28}O_{46}$ hexaferrite samples heated at 900 °C for 5 h, prepared with and without the presence of different weight ratios of *ginger* root extract: (a) Sample (A), (b) Sample (B), (c) Sample (C), (d) Sample (D), and (e) Sample (E).

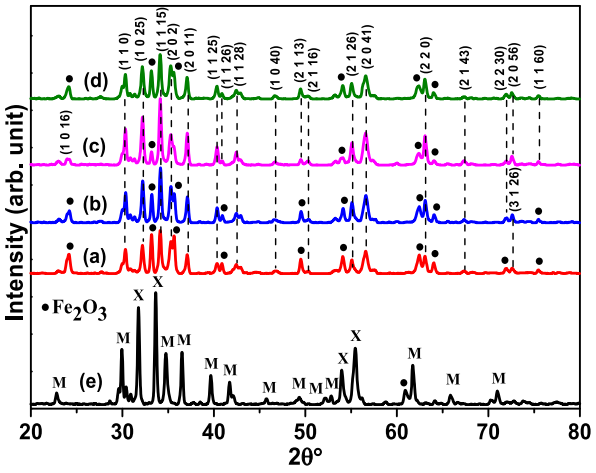

Fig. 3. XRD patterns of X-type $Ba_2Zn_2Fe_{28}O_{46}$ hexaferrite samples heated at 900 °C for 5 h, prepared with and without the presence of different weight ratios of *ginger* root extract: (a) Sample (A), (b) Sample (B), (c) Sample (C), (d) Sample (D), and (e) Sample (E) (Fe_2O_3 - Hematite phase, M- M type ferrite phase and X-X type ferrite phase).

3. Results and discussions

3.1. FTIR analysis

Fig. 2 shows the FTIR spectra of $Ba_2Zn_2Fe_{28}O_{46}$ hexaferrite powder synthesised with and without the presence of *ginger* root extract and heated at 900 °C for 5 h (Sample (A-E)). The absorption bands in the FTIR spectra at 584 cm^{-1} and 434 cm^{-1} are assigned to the tetrahedral (ν_1) and octahedral (ν_2) metal-oxygen bond vibrations of the crystal lattice, and are characteristic of hexagonal ferrites [42]. Absorption bands in the wavenumber range 434–439 cm^{-1} (ν_2) are assigned to the Fe–O stretching of Fe–O_6, while, the bands in the wavenumber range 580–585 cm^{-1} (ν_1) are assigned to the Fe–O stretching of Fe–O_4 [43]. All heated samples show a small absorption band at ~1632 cm^{-1}, indicating the O–H stretching vibrations which may be due to the polyol [44]. However, the sample prepared without ginger root extract shows a broad (strong) absorption peak between 3300 and 3600 cm^{-1}, which is due to the stretching vibration of an O–H bond [45,46], and is typical of water. The fact that this is absent in the samples with *ginger* (Sample (A-D), Fig. 2a-d) suggests that the sample without *ginger* (Sample (E), Fig. 2e) is much more hygroscopic and has absorbed atmospheric moisture much more rapidly after cooling.

3.2. XRD analysis

XRD patterns of X-type $Ba_2Zn_2Fe_{28}O_{46}$ hexaferrite samples were indexed using the standard patterns for X-type ($Ba_2Me_2Fe_{28}O_{46}$) hexagonal crystals (JCPDS # 01-073-2034), and are shown in Fig. 3. XRD analysis of the samples, prepared in the presence of different weight ratios of *ginger* root extract and heated at 900 °C for 5 h revealed the formation of X-type ferrite and hematite (α-Fe_2O_3) (JCPDS # 04-015-9569) as a minor secondary phase. However, the sample prepared without *ginger* root extract (Sample (E)) shows the formation of a mixture of phases: 72.2% of M-type ferrite ($BaFe_{12}O_{19}$) (JCPDS # 84–0757), only 22.2% X-type, and 5.6% hematite. Therefore, the addition of the *ginger* root extract has enabled the formation of a single hexaferrite phase (X-type) at a low temperature of only 900 °C, with non-magnetic α-Fe_2O_3 as a minor secondary phase. The phase composition values are given in Table 1.

It can be seen from Fig. 3 that the sample prepared with 52.5 g weight of *ginger* root extract (Sample (C), Fig. 3c) contained the lowest amount of hematite compared to the others, with 82.61% X ferrite, while the quantity of hematite increased again when the weight ratio of *ginger* root extract increased to 70 g (Sample (D), Fig. 3d), yielding 75.0% X ferrite. Therefore, the XRD patterns confirmed that 52.5 g weight of *ginger* root extract (Sample (C), Fig. 3c) was the optimum for the synthesis of X-type ($Ba_2Zn_2Fe_{28}O_{46}$) hexaferrites.

The variation of lattice constants and unit cell volume with different weight ratios of *ginger* root extract is shown in Fig. 4 and Table 1. The average crystallite size was investigated from the most intense peak using the following Scherrer formula [47].

$$D_{(xrd)} = \frac{K\lambda}{\beta cos\theta} \quad (1)$$

where K is a dimensionless shape factor and has a value about of 0.9 which varies with the actual shape of the crystallite; λ is the X-ray wavelength (1.5406 Å); θ is the angle of Bragg diffraction, and β is the full width at half the maximum intensity. The obtained structural parameters are listed in Table 1. The crystallite size of all samples, heated at 900 °C for 5 h varies in the range of 28–37 nm.

The unit cell volume was calculated using the following equation.

$$V = a^2c \sin 120° \quad (2)$$

where 'V' is the volume of the unit cell and 'a' and 'c' are the lattice constants.

The crystallite size was ~37 nm without *ginger* extract, and between 28-31 nm in all cases with *ginger* extract, suggesting that the reducing agent had the effect of slightly lowering crystallite size in the ferrites produced. Similarly, the lattice parameters and cell volume were larger, for all samples produced with *ginger* root extract compared to that without.

The values of bulk density (d_B) and X-ray density (D_x) were calculated using the following equations [48].

$$d_B = \frac{m}{\pi r^2 h} \quad (3)$$

$$D_x = \frac{3M}{Na^2c} \quad (4)$$

where m is mass of pellet, r is a radius of pellet, h is the height

Table 1
Structural parameters of X-type $Ba_2Zn_2Fe_{28}O_{46}$ hexaferrite samples prepared without and with the different weight ratio of *ginger* root extract and heated at 900 °C for 5 h.

Code	Lattice parameters		Cell volume V (Å^3) (±5)	Crystallites size D_{xrd} (nm) (±0.2)	FWHM (deg.)	% of X-phase (±0.1)	% of α-Fe_2O_3 (±0.1)	% of M-phase (±0.1)
	a (Å) (±0.02)	c (Å) (±0.2)						
Sample (A)	5.889	86.303	2592.03	29.30	0.2964	58.33	41.67	–
Sample (B)	5.889	86.308	2592.18	31.34	0.2771	62.50	37.50	–
Sample (C)	5.888	86.310	2591.35	30.15	0.2880	82.61	17.39	–
Sample (D)	5.889	86.310	2592.24	27.91	0.3111	75.00	25.00	–
Sample (E)	5.760	82.100	2358.88	36.95	0.2350	22.22	5.56	72.22

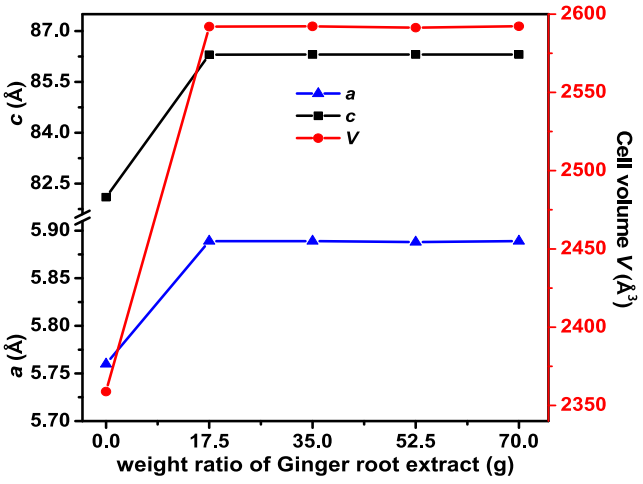

Fig. 4. Variation of lattice constants (a, c) and unit cell volume (V) of $Ba_2Zn_2Fe_{28}O_{46}$ hexaferrite samples prepared without *ginger* root extract and with different weight ratios of *ginger* root extract heated at 900 °C for 5 h (Sample (A–D)).

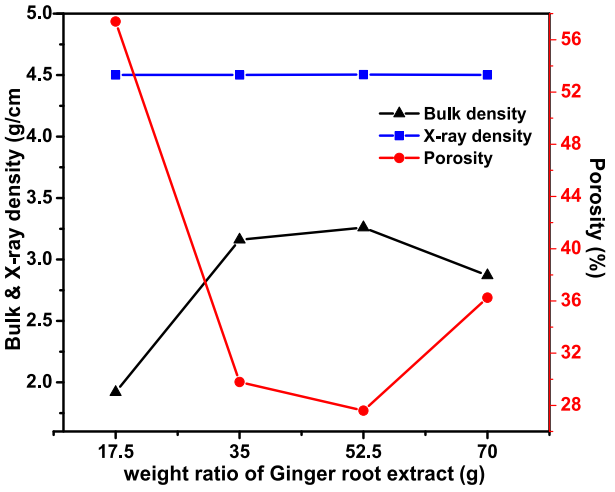

Fig. 5. Variation of the bulk density, X-ray density, and porosity of $Ba_2Zn_2Fe_{28}O_{46}$ hexaferrite samples prepared with the different weight ratios of *ginger* root extract heated at 900 °C for 5 h (Sample (A–D)).

(thickness) of pellet, M is molecular weight, a and c are lattice constants, and N is Avogadro's number (6.02×10^{23}/mole).

The value of porosity for all samples is calculated using the following equation.

$$P = (1 - \frac{d_B}{D_x}) \times 100\% \quad (5)$$

The calculated values of X-ray density, bulk density and porosity of all the samples heated at 900 °C for 5 h are shown in Table 2. The value of bulk density varies in the range of 1.90–3.30 g/cm^3 (Table 2). The sample prepared with 52.5 g *ginger* root extract (Fig. 3c), that contained the most X-ferrite phase (82.61 %), also had the minimum value of porosity and maximum value of bulk density. However, as these pellets were only heated to 900 °C, hence they are very poorly sintered and are not close to the maximum density possible (5.313 g/cm^3). The calculated X-ray densities were higher, at ~4.50 g/cm^3 (see Table 2).

Fig. 5 shows the variation in bulk density (d_B), X-ray density (D_x) and porosity (P) with the different weight ratios of *ginger* root extract for the samples heated at 900 °C for 5 h.

Fig. 6 shows the SEM micrographs (1 μm scale bar) for all the samples (Sample (A-D)) showing the grain morphology of prepared hexaferrites. It is observed from micrographs that the grains are agglomerated and are irregular in shape. As the weight ratio of *ginger* root extract increases, porosity decreases, and agglomeration increases. The sample prepared in presence of 17.5 g *ginger* root extract (Sample (A), Fig. 6a) possesses spongy structure and it also possesses a high value of porosity (57.40%) and low value of bulk density (1.92 g/cm^3) compared to all other samples.

3.3. Magnetic properties

The hysteresis loops of $Ba_2Zn_2Fe_{28}O_{46}$ samples prepared in the presence of *ginger* root extract, heated at 900 °C were recorded on a VSM under an applied magnetic field of ±1.0 T and shown in Fig. 7. The different magnetic parameters such as saturation magnetisation (M_S), remanent magnetisation (M_r), coercivity (H_C), and squareness ratio (M_r/M_S) of prepared hexaferrites are calculated from the M – H loops and their values are listed in Table 3.

The values of saturation magnetisation (M_S) and remanent

Table 2
The bulk density, X-ray density, and the porosity of $Ba_2Zn_2Fe_{28}O_{46}$ hexaferrite samples heated at 900 °C for 5 h.

Code	Bulk density d_B (g/cm^3) (±0.01)	X-ray density D_x (g/cm^3) (±0.02)	Porosity P (%) (±0.1)
Sample (A)	1.92	4.502	57.40
Sample (B)	3.16	4.502	29.79
Sample (C)	3.26	4.504	27.60
Sample (D)	2.87	4.502	36.25

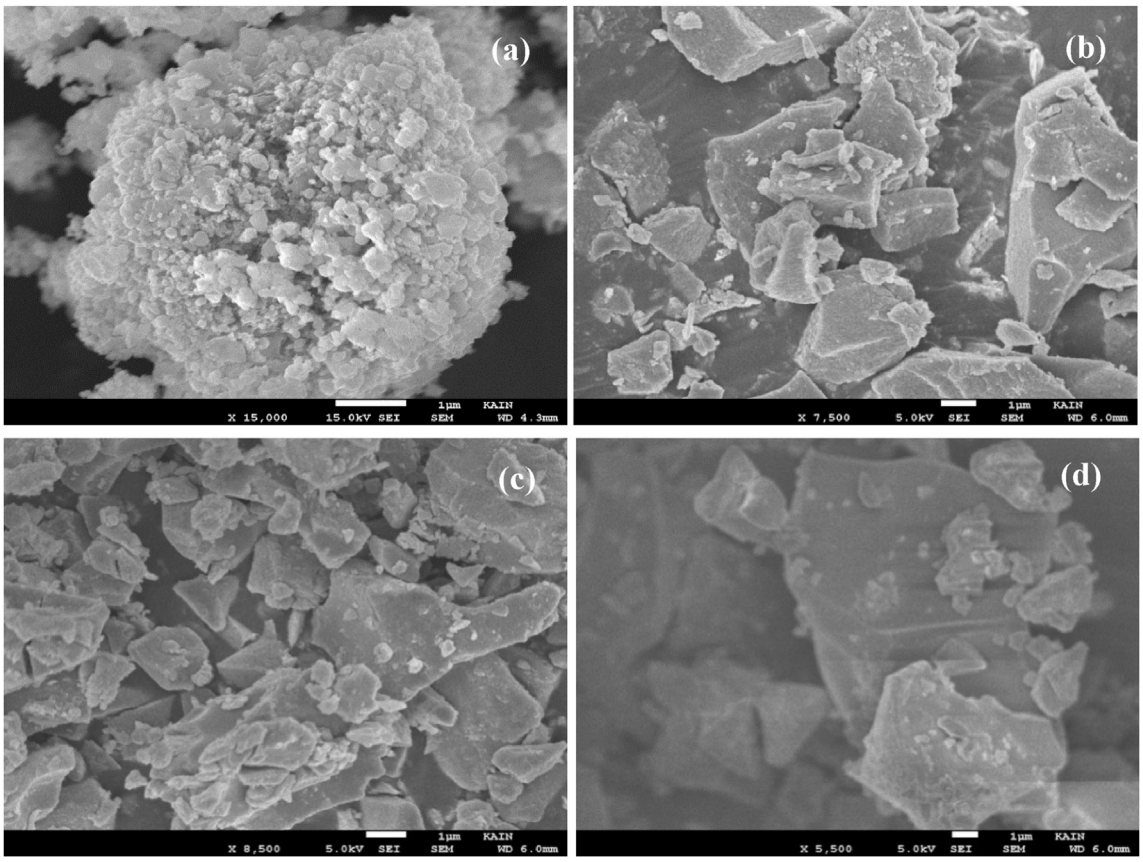

Fig. 6. SEM images (1 μm scale bar) of $Ba_2Zn_2Fe_{28}O_{46}$ hexaferrite samples heated at 900 °C for 5 h, prepared with the presence of different weight ratios of *ginger* root extract: (a) Sample (A), (b) Sample (B), (c) Sample (C), (d) Sample (D).

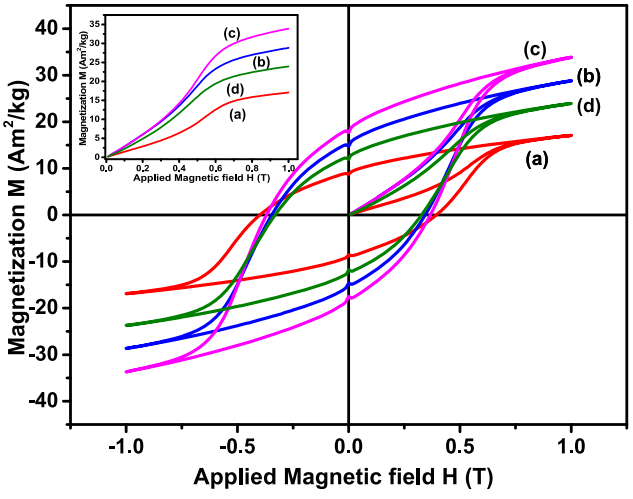

Fig. 7. M – H loops and initial magnetisation curves (inset) of $Ba_2Zn_2Fe_{28}O_{46}$ hexaferrite samples heated at 900 °C for 5 h, prepared with the different weight ratios of *ginger* root extract: (a) Sample (A), (b) Sample (B), (c) Sample (C), (d) Sample (D).

magnetisation (M_r) increase as the weight ratio of *ginger* root extract increases except for the sample prepared with 70.0 g *ginger* root extract (Sample (D)), that had a lower X-ferrite content than that with 52.5 g, as shown in Table 3. The value of coercivity lies in the range of 262.6–318.3 kA m^{-1} (0.33–0.40 T = 3300–4000 Oe) in all cases, which shows that the prepared samples belong to the family of hard ferrites [49], as would be expected for $Ba_2Zn_2Fe_{28}O_{46}$.

The variation of saturation magnetisation (M_S), remanent magnetisation (M_r) and coercivity (H_c) with the different weight ratios of *ginger* root extract are shown in Fig. 8 (a).

In the present study, the sample prepared with 52.5 g *ginger* root extract (Sample (C)) possesses the highest value of saturation magnetisation (M_S = 33.87 Am^2 kg^{-1} or emu/g) in comparison with the remaining prepared samples. This is because this sample exhibits the maximum amount of X-phase (82.61%). The variation in M_S follows the trend of X-phase present in the sample as shown in Fig. 8 (b). This M_S value (33.87 Am^2 kg^{-1} or emu/g) is particularly low in comparison with the reported maximum value of saturation magnetisation (M_S = 73.1 Am^2 kg^{-1} or emu/g) [50]. The low value of M_S is partially attributed to the presence of the antiferromagnetic phase of hematite (17.39% of α- Fe_2O_3) [51,52], as confirmed by XRD analysis (Fig. 3), as a sample containing only 82.61 wt % X ferrite would be expected to have a M_S value of 60.39 Am^2 kg^{-1}. The fact that the value here is still only around half of this value could be explained by the low synthesis temperature (900 °C) used here – magnetisation is known to increase as synthesis/sintering temperature increases, and the low crystallite size seen in these samples is well below the typical maximum magnetic domain sizes reported for hexaferrites of between 0.5 μm and 1 μm [1]. The squareness ratio (M_r/M_S) is also calculated from the values of M_r and M_S and their values are tabulated in Table 3. Previously, it has been reported that the squareness ratio of hexaferrite samples equal or above 0.5 shows that the material possesses a single magnetic domain and below 0.5 shows the formation of a multi-domain structure [52a, 52b]. In the present study, the squareness ratio of all the samples is in the range of 0.511–0.570 (Table 3) showing that all the samples possess a single domain structure.

Table 3
Magnetic parameters of $Ba_2Zn_2Fe_{28}O_{46}$ hexaferrites prepared with the different weight ratios of *ginger* root extract and heated at 900 °C for 5 h.

Sr. No.	Code	Remanence Magnetisation M_r ($Am^2\ kg^{-1}$)	Saturation Magnetisation M_S ($Am^2\ kg^{-1}$)	Squareness ratio M_r/M_S	Coercivity H_C (T)	H_a (kA m^{-1})	H_a (Oe)
1	Sample (A)	8.75	17.08	0.5122	0.40	149.71	1881.25
2	Sample (B)	14.75	28.86	0.5110	0.35	156.73	1969.47
3	Sample (C)	17.66	33.87	0.5214	0.38	147.17	1849.34
4	Sample (D)	11.92	20.92	0.5698	0.33	108.10	1358.38

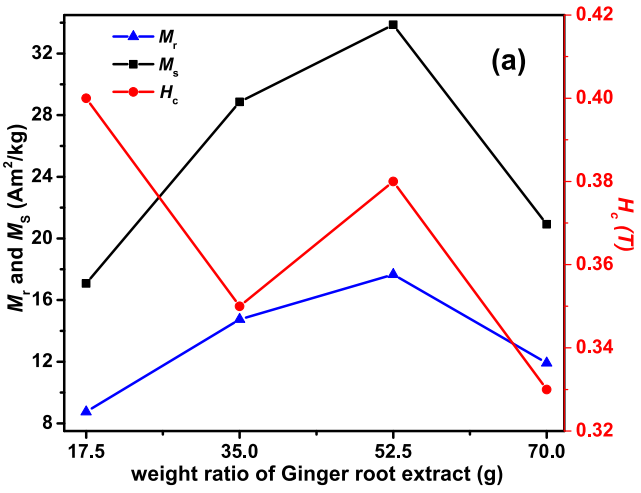

Fig. 8. (a) Variation in saturation magnetisation (M_S), remanent magnetisation (M_r), coercivity (H_c) and, (b) Relative percentage of two phases of $Ba_2Zn_2Fe_{28}O_{46}$ hexaferrite samples prepared with the different weight ratios of *ginger* root extract heated at 900 °C for 5 h (Sample (A–D)).

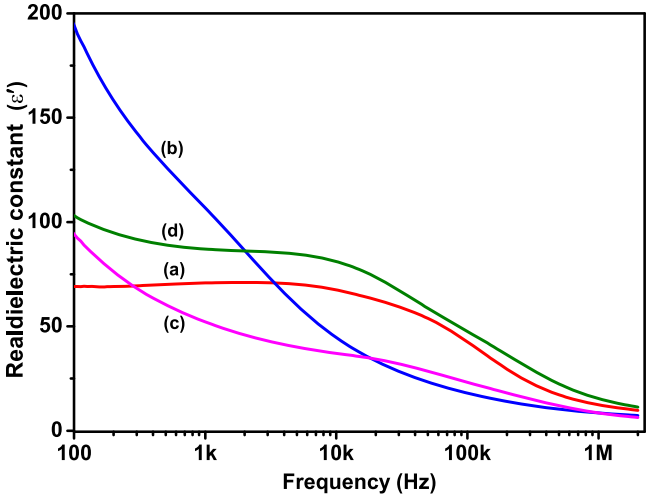

Fig. 9. Variation in real dielectric constant (ε′) of $Ba_2Zn_2Fe_{28}O_{46}$ hexaferrite samples heated at 900 °C for 5 h, prepared with the different weight ratios of *ginger* root extract: (a) Sample (A), (b) Sample (B), (c) Sample (C), (d) Sample (D).

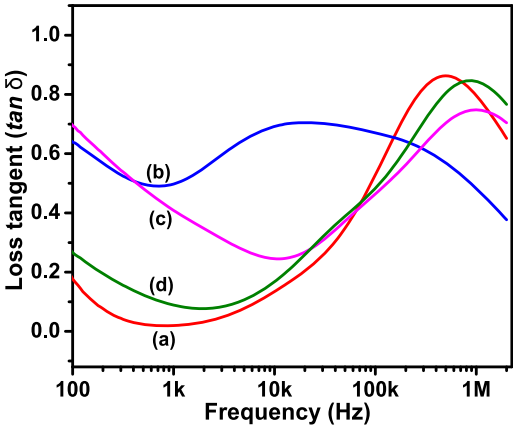

Fig. 10. Variation in loss tangent (*tan δ*) as a function of frequency for $Ba_2Zn_2Fe_{28}O_{46}$ hexaferrite samples heated at 900 °C for 5 h, prepared with the different weight ratios of *ginger* root extract: (a) Sample (A), (b) Sample (B), (c) Sample (C), (d) Sample (D).

3.4. Dielectric properties

It is observed from Fig. 9 that at low-frequency, the dielectric constant of the sample prepared with 35 g *ginger* root extract (Sample (B)) decreases rapidly and approaches a constant above 1 MHz, while the other samples (Sample (A), (C) and (D)) show lower initial permittivity, and resonance peaks at around 10–50 kHz. This decrease in dielectric constant with frequency is a normal behaviour of most ferri-magnetic materials and has also been observed by several other researchers [53–55]. This behaviour of dielectric dispersion can be explained based on Koop's phenomenological theory, which is based on the Maxwell-Wagner interfacial polarisation model [56]. According to this model, the dielectric medium of ferrite consists of two layers. The first layer of fairly well-conducting boundaries is separated by the second layer of relatively poor conducting boundaries. The first layer is strongly effective at higher frequencies, while the second layer is dominant at lower frequencies. The free electrons reach the grain boundaries through hopping [57] and 'pile-up' at the grain boundaries if the grain boundaries' resistance is high enough and, hence, produce induced polarisation. In ferrites, the polarisation is a similar process to that of the conduction process. The free electrons in a dielectric medium need a finite time to line up their axes in the direction of

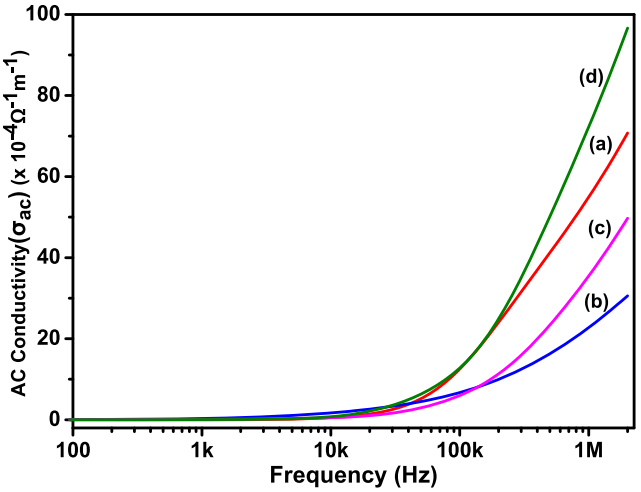

Fig. 11. Variation of ac conductivity with frequency of $Ba_2Zn_2Fe_{28}O_{46}$ hexaferrite samples heated at 900 °C for 5 h, prepared with the different weight ratio of *ginger* root extract: (a) Sample (A), (b) Sample (B), (c) Sample (C), (d) Sample (D).

the applied field. If the frequency of the applied field is increased, free electrons cannot align with the applied field at a certain point and hence cannot follow the changes in the applied field over a certain frequency range [58]. As a result, the probability of free electrons reaching grain boundaries is decreased and the free electron polarisation virtually does not contribute to the polarisation that decreases the dielectric constant [56,59].

Fig. 10 shows the variation of loss tangent (*tan* δ) of all the prepared samples (Sample (A-D)) with frequency at room temperature. The value of loss tangent depends on different factors such as Fe^{+2} content, structural homogeneity, stoichiometry ratio, preparation time and heating temperature [60]. The value of loss tangent decreases with increasing frequency, that is because beyond a certain frequency limit hopping frequency of charge between Fe^{3+} and Fe^{2+} cannot follow the frequency of the applied electric field. The sample prepared with 35 g ginger root extract (Sample (B)) shows a broad resonance peak between 10 kHz and 100 kHz, while other samples show resonance between 300 kHz and 2 MHz frequency range.

AC conductivity (σ_{ac}) of the samples was calculated by the formula [61];

$$\sigma_{ac} = 2\pi f\, \varepsilon_0 \varepsilon'' \quad (6)$$

Where ε_0 is permittivity of free space and, ε'' is dielectric loss.

The variation of ac conductivity of all the hexaferrite samples (Sample (A-D)) with frequency (100 Hz - 2 MHz) at room temperature is shown in Fig. 11. It can be observed from Fig. 11 that ac conductivity increases with the increase of frequency, which is because increment in frequency increases the hopping frequency of the charge carriers between Fe^{2+} and Fe^{3+}.

3.4.1. Frequency-dependent impedance

The real part of impedance (Z′) and complex part of impedance (Z″) as a function of applied field frequency in the range of 10 Hz to 2 MHz for X-type, $Ba_2Zn_2Fe_{28}O_{46}$ hexaferrite samples heated at 900 °C for 5 h measured at room temperature are shown in Fig. 12 and Fig. 13, respectively.

It can be seen from Figs. 12 and 13 that the real part of impedance (Z′) and complex part of impedance (Z″) for all different weight ratios of *ginger* root extract decreases fast as frequency increases. Their values become almost constant beyond 300 Hz frequency that shows no dependency of Z′ and Z″ on frequency.

3.4.2. Electric modulus analysis

Analysis of electric modulus is very important to understand the various parameters of electrical transport performance such as the rate of ion hopping and conductivity relaxation time contribution to the conductivity of the prepared hexaferrite material [62].

Fig. 14 (a) shows the variation of the real part of the electric modulus (M') of samples heated at 900 °C as a function of

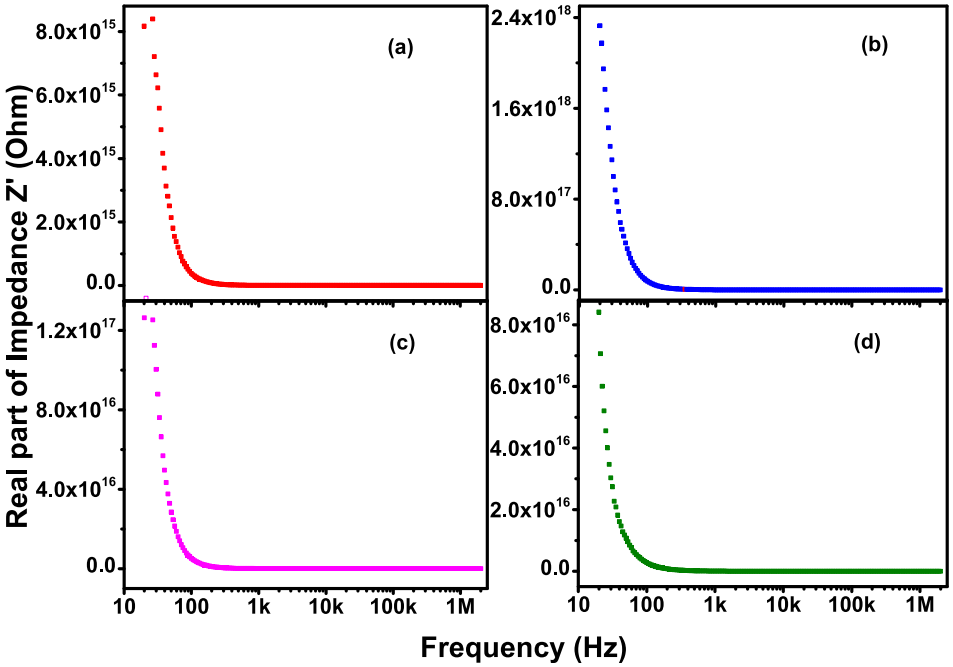

Fig. 12. Variation of the real part of impedance (Z′) with frequency for X-type $Ba_2Zn_2Fe_{28}O_{46}$ hexaferrite samples heated at 900 °C for 5 h, prepared with the different weight ratios of *ginger* root extract: (a) Sample (A), (b) Sample (B), (c) Sample (C), (d) Sample (D).

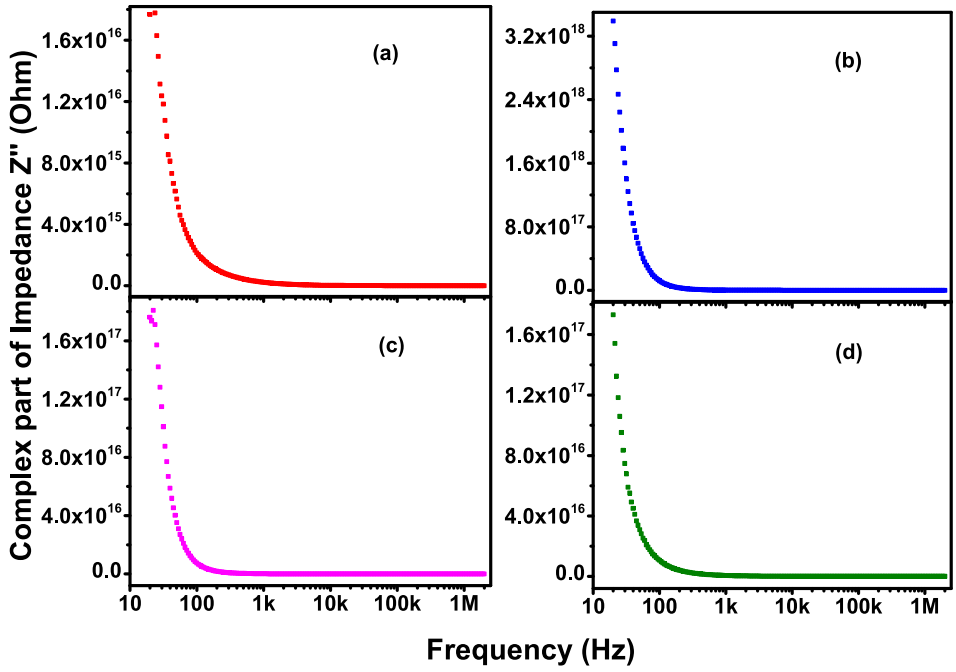

Fig. 13. Variation of the complex part of impedance (Z″) with frequency for X-type, $Ba_2Zn_2Fe_{28}O_{46}$ samples heated at 900 °C for 5 h, prepared with the different weight ratios of *ginger* root extract: (a) Sample (A), (b) Sample (B), (c) Sample (C), (d) Sample (D).

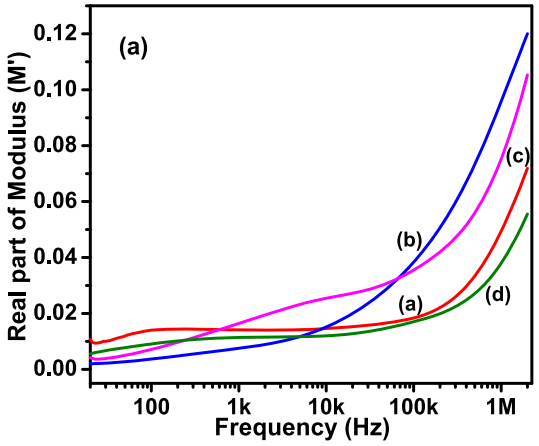

Fig. 14a. Variation in the real part of electric modulus as a function of frequency for $Ba_2Zn_2Fe_{28}O_{46}$ hexaferrite samples heated at 900 °C for 5 h, prepared with the different weight ratios of *ginger* root extract: (a) Sample (A), (b) Sample (B), (c) Sample (C), (d) Sample (D).

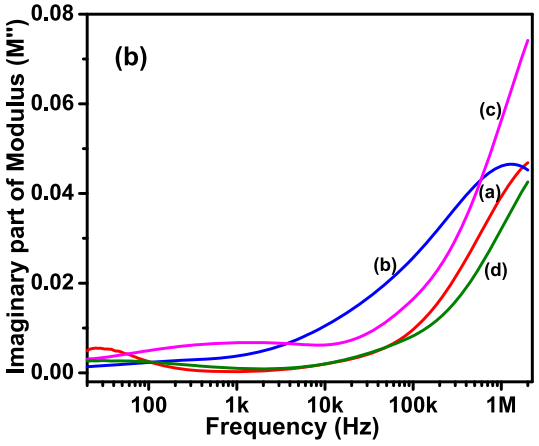

Fig. 14b. Variation in the imaginary part of electric modulus as a function of frequency for $Ba_2Zn_2Fe_{28}O_{46}$ hexaferrite samples heated at 900 °C for 5 h, prepared with the different weight ratios of *ginger* root extract: (a) Sample (A), (b) Sample (B), (c) Sample (C), (d) Sample (D).

frequency. It can be observed from Fig. 14 (a) that at low frequency, the value of real electric modulus (M′) of all samples prepared in presence of ginger root extract (Sample (A-D)) is low and at the high-frequency region, it increases very fast. When the electric field is applied, it decreases the restoring force between the charge carriers, which is responsible for the high value of M′ at the high-frequency region [63]. The maximum value of real modulus (M'~0.12 at 2 MHz) is observed in the sample prepared with 35.0 g *ginger* root extract (Sample (B)).

The variation of imaginary part of the electric modulus (M″) for all samples heated at 900 °C (Sample (A-D)) is shown in Fig. 14 (b) as a function of frequency. The present graph explains the brief information about the charge transport mechanism, such as ion dynamics, conductivity relaxation and electrical transport mechanism as a function of the frequency [62]. The maximum value (M" ~0.075 at 2 MHz) is observed in the sample prepared with 52.5 g ginger root extract (Sample (C)). The relaxation peak is observed around 1 MHz in the sample prepared with 35.0 g *ginger* root extract (Sample (B)) due to the mobility of charge carriers. Below the relaxation peak, the charge carriers are mobile and above the relaxation peak, the charge carriers are immobile, which confined to a potential well [64].

Cole-Cole type plots provide information about the grains, grains boundary effects; are plotted and shown in Fig. 15. The Cole-Cole type plot (Nyquist plot) of electric modulus analysis is more helpful than impedance analysis (Z″ versus Z′). This analysis accurately separates the relaxation effects from grain and grain boundary in ferrite material. The imaginary part of impedance (Z″) gives the relaxation dynamics from largest resistance of the material, while, the imaginary part of the modulus (M″) gives the

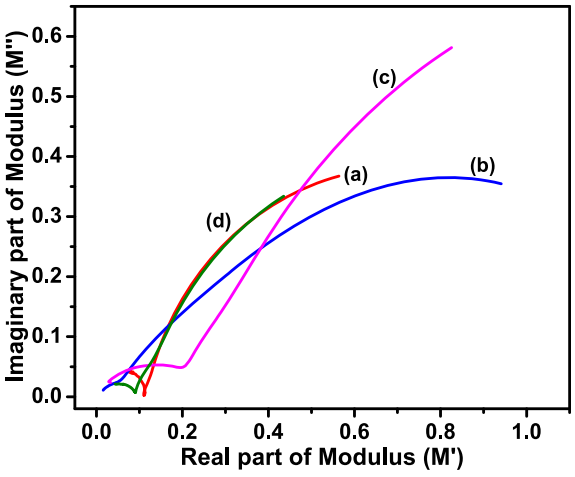

Fig. 15. Cole-Cole type plots of $Ba_2Zn_2Fe_{28}O_{46}$ hexaferrite samples heated at 900 °C for 5 h, and prepared with the different weight ratios of *ginger* root extract:: (a) Sample (A), (b) Sample (B), (c) Sample (C), (d) Sample (D).

smallest capacitance (i.e. the highly conductive part) of the material [65]. It can be observed from Fig. 15 that all samples (Sample (A-D)) show semicircle arc in the low-frequency region attributed to the grain resistance [66]. The sample prepared with 52.5 g ginger root extract. Sample (C) shows semicircle at the low-frequency region, that indicates the relaxation phenomena with different relaxation time (τ), associated with each relaxation. The capacitance (C) value can be calculated at the maximum frequency (f_{max}) using the following relation [67]:

$$M'' = (\varepsilon_o / 2C) \quad (7)$$

Where ε_0 is permittivity of free space.

4. Conclusions

X-type Barium zinc hexaferrite $Ba_2Zn_2Fe_{28}O_{46}$ powder has been successfully synthesised using the combustion treatment method at 900 °C for 5 h in presence of different weight ratios of *ginger* root extract. From XRD analysis it has been found that the sample prepared with 52.5 g *ginger* root extract, heated at 900 °C contained maximum amount (82.61 %) of X-phase with less impurity of hematite (17.39%) compared to other samples heated at 900 °C. The sample prepared with 52.5 g *ginger* root extract possesses the highest value of saturation magnetisation ($M_S = 33.87$ Am^2 kg^{-1}) in comparison with the other prepared samples, and all were hard ferrites with a single domain structure. The sample prepared with 35 g ginger root extract shows a broad loss tangent resonance peak between 10 kHz and 100 kHz, while other samples show loss tangent resonance peaks between 300 kHz and 2 MHz frequency range.

Declaration of competing interest

The authors declare that they have not known to competing financial interest or personal relationship that could appeared to influence to work reported to this paper.

CRediT authorship contribution statement

Amrin R. Kagdi: Samples preparation, sample characterisation, Preparing original draft, Formal analysis, Data curation, Software, plotting graphs. **Robert C. Pullar:** Sample characterisation, review & editing, draft modification, Validation, Conceptualization, Visualization, Funding acquisition, English and grammar checking, Final draft checking and modification. **Sher Singh Meena:** Sample characterisation, Formal analysis, draft modification, review & editing, Proof reading .**Rajshree B. Jotania:** Supervision, Methodology, review, modification & editing, Investigation, Data curation, Project administration, Proof reading .**Khalid Mujasam Batoo:** Sample characterisation, modification & editing draft, Funding acquisition, Formatting references.

Acknowledgments

This work was supported by DRS—SAP (Phase-II, F-530/17/DRS-II/2018 (SAP-I)) grant, New Delhi, India and DST—FIST (level- I, No. SR/FST/PSI-198/2014) grant, India. One of the authors (Amrin R. Kagdi) acknowledges the Ministry of Minority Affairs, Govt. of India for providing Maulana Azad National Fellowship (No. F1—17.1/2013—14/MANF—2013—14—MUS—GUJ—28541). R. C. Pullar wishes to thank National funding provided by FCT (Fundação para a Ciência e a Tecnologia, Portugal) grant IF/00681/2015, and this work was developed within the scope of the project CICECO-Aveiro Institute of Materials, UIDB/50011/2020 & UIDP/50011/2020, financed by national funds through the FCT/MCTES. K. M. Batoo is thankful to Researchers Supporting Project (RSP-2019/148) at King Saud University for financial support.

References

[1] R.C. Pullar, Hexagonal Ferrites a review of the synthesis, properties and applications of hexaferrite ceramics, Prog. Mater. Sci. 57 (2012) 1191—1334.
[2] S. Malhotra, M. Chitkara, I.S. Sandhu, Naini Dawar, J. Singh, Investigation of structural, magnetic and dielectric properties of terbium doped strontium hexaferrite for high frequency applications, Ind. J. Sci. Techn. 9 (2016) 96638.
[3] D.L. Leslie-Pelecky, R.D. Rieke, Magnetic properties of nanostructured materials, Chem. Mater. 8 (1996) 1770—1783.
[4] F.J. Himpsel, J.E. Ortega, G.J. Mankey, R.F. Willis, Magnetic nanostructures, Adv. Phys. 47 (1998) 511—597.
[5] M. Sugimoto, The past, present and future of ferrites, J. Am. Ceram. Soc. 82 (1999) 269—280.
[6] G. Bate, Magnetic recording materials since 1975, J. Magn. Magn Mater. 100 (1991) 413—424.
[7] A. Jordan, R. Scholz, P. Wust, H. Schirra, T. Schiestel, H. Schmidt, R. Felix, Endocytosis of dextran and silan-coated magnetite nanoparticles and the effect of intracellular hyperthermia on human mammary carcinoma cells in vitro, J. Magn. Magn Mater. 194 (1999) 185—196.
[8] D.H. Kim, D.E. Nikles, D.T. Johnson, C.S. Brazel, Heat generation of aqueously dispersed $CoFe_2O_4$ nanoparticles as heating agents for magnetically activated drug delivery and hyperthermia, J. Magn. Magn Mater. 320 (2008) 2390—2396.
[9] S. Mornet, S. Vasseur, F. Grasset, E. Duguet, Magnetic nanoparticle design for medical diagnosis and therapy, J. Mater. Chem. 14 (2004) 2161—2175.
[10] S. Wada, K. Tazawa, I. Furuta, H. Nagae, Antitumor effect of new local hyperthermia using dextran magnetite complex in hamster tongue carcinoma, Oral Dis. 9 (2003) 218—223.
[11] M.D. Shultza, S. Calvin, P.P. Fatouros, S.A. Morrison, E.E. Carpenter, Enhanced ferrite nanoparticles as MRI contrast agents, J. Magn. Magn Mater. 311 (2007) 464—468.
[12] L. Zhen, K. He, C.Y. Xu, W.Z. Shao, Synthesis and characterization of single crystalline $MnFe_2O_4$ nanorods via a surfactant-free hydrothermal route, J. Magn. Magn Mater. 320 (2008) 2672—2675.
[13] S.R. Pezeshki, M.W. Hester, Q. Lin, J.A. Nyman, The effects of oil spill and clean-up on dominant US Gulf coast marsh macrophytes: a review, Environ. Pollut. 108 (2000) 129—139.
[14] J.A. Dahl, B.L.S. Maddux, J.E. Hutchison, Toward greener nanosynthesis, Chem. Rev. 107 (2007) 2228—2269.
[15] M. Sastry, A. Ahmad, M.I. Khan, R. Kumar, C.M. Niemeyer, C.A. Mirkin (Eds.), Microbial Nanoparticle Production, Wiley-VCH, Weinheim, Germany, 2004, pp. 126—135.
[16] A. Chakraborty, D.K. Das, M. Sinha, S. Dey, S. Bhattacharjee, Moringa oleifera leaf extract mediated green synthesis of stabilized gold nanoparticles, J. Bionanoscience 7 (2013) 415—419.
[17] S. Sathya, S. Parthasarathi, V. Murugan, S. Ramesh, Y. Kyusik, Biogenic synthesis of multidimensional gold nanoparticles assisted by *Streptomyces hygroscopicus* and its electrochemical and antibacterial properties, Biometals 25 (2012) 351—360.
[18] G. Rishalan, P. Alisa, R.M. Gengan, K. Anand, A.A. Chuturgoon, Silver

nanoparticles of *Albizia adianthifolia*: the induction of apoptosis in human lung carcinoma cell line, J. Nanobiotechnol. 11 (5) (2013) 1–9.
[19] B.V. Tirupanyam, Ch Srinivas, S.S. Meena, S.M. Yusuf, A. Satish Kumar, D.L. Sastry, V. Seshubai, Investigation of structural and magnetic properties of co-precipitated Mn–Ni ferrite nanoparticles in the presence of α-Fe_2O_3 phase, J. Magn. Magn Mater. 392 (2015) 101–106.
[20] P. Kaur, S.K. Chawla, S.S. Meena, S.M. Yusuf, K. Pubby, S.B. Narang, Synthesis of Co-Zr doped nanocrystalline strontium hexaferrites by Sol–Gel auto-combustion route using sucrose as fuel and study of their structural, magnetic and electrical properties, Ceram. Int. 43 (2017) 590–598.
[21] S.K. Chawla, R.K. Mudsainiyan, S.S. Meena, S.M. Yusuf, Sol-gel synthesis, structural and magnetic properties of nanoscale M-type barium hexaferrites BaCoxZrxFe(12−2x)O19, J. Magn. Magn Mater. 350 (2014) 23–29.
[22] M. Hashim, S.E. Shirsath, S.S. Meena, M.L. Mane, S. Kumar, P. Bhatt, R. Kumar, N.K. Prasad, S.K. Alla, J. Shah, R.K. Kotnala, K.A. Mohammed, E. Senturk, Alimuddin, Manganese ferrite prepared using reverse micelle process: structural and magnetic properties characterization, J. Alloys Compd. 642 (2015) 70–77.
[23] J. Singh, C. Singh, D. Kaur, H. Zaki, I.A. Abdel-Latif, S. BindraNarang, R. Jotania, S.R. Mishra, R. Joshi, P. Dhruv, M. Ghimire, S.E. Shirsath, S.S. Meena, Elucidation of phase evolution, microstructural, Mossbauer and magnetic properties of Co 2þ eAl 3þ doped M-type BaSr hexaferrites synthesized by a ceramic method, J. Alloys Compd. 695 (2017) 1112–1121.
[24] S.C. Bhargava, H. Kunkel, S. Singh, A.H. Morrish, Z.W. Li, Spin glass ordering of Zn0.75Co0.25Fe0.5Cr1.5O4 cubic spinel, Solid State Commun. 126 (2003) 535–540.
[25] V. Parashar, R. Prashar, B. Sharma, A.C. Pandey, Parthenium leaf extract mediated synthesis of silver nanoparticles: a novel approach towards weed utilization, Dig. J. Nanomater. Biostruct. 4 (2009) 45–50.
[26] N. Saifuddin, C.W. Wong, A.A. Nuryusumina, Rapid biosynthesis of silver nanoparticles using culture supernatant of bacteria with microwave irradiation, J. Chem. 6 (2009) 61–70.
[27] K.C. Bhansa, S.F. D Souza, Extracellular biosynthesis of silver nanoparticles using the fungus Aspergillus fumigates, Colloids Surf. B Biointerfaces 47 (2006) 160–164.
[28] K. Chaieb, H. Hajlaoui, T. Zmantar, A.B. Kahla-Nakbi, M. Rouabhia, K. Mahdouani, A. Bakhruf, The chemical composition and biological activity of clove essential oil, eugenia caryophyllata (syzigium aromaticum L. Myrtaceae): a short review, Phyther. Res. 21 (2007) 501–506.
[29] S.T. Chang, P.F. Chen, S.C. Chang, Antibacterial activity of leaf essential oil sand their constituents from Cinnamomum osmophloeum, J. Ethnopharmacol. 77 (2001) 123–127.
[30] H.K. Kwon, W.K. Jeon, J.S. Hwang, C.G. Lee, J.S. So, J.A. Park, et al., Cinnamon extract suppresses tumor progression by modulating angiogenesis and the effector function of CD8+T cells, Canc. Lett. 278 (2009) 174–182.
[31] B.H. Ali, G. Blunden, M.O. Tanira, A. Nemmar, Some phytochemical, pharmacological and toxicological properties of ginger (Zingiber officinale Roscoe): a review of recent research, Food Chem. Toxicol. 46 (2008) 409–420.
[32] A.M. Bode, Z. Dong, The Amazing and Mighty Ginger, Herbal Medicine: Biomolecular and Clinical Aspects, second ed., CRC Press, Taylor & Francis, 2011.
[33] I.T. Carvalho, L. Santos, Antibiotics in the aquatic environments: a review of the European scenario, Envirom. Intern. 94 (2016) 736–757.
[34] Y. Sakai, H. Nagase, Y. Ose, T. Sato, M. Kawai, M. Mizuno, Effects of medicinal plant extracts from Chinese herbal medicines on the mutagenic activity of benzo(a)pyrene, Mutat. Res. 206 (1988) 327–334.
[35] A.H. Rahmani, F. M. Al Shabrmi, S.M. Aly, Active ingredients of ginger as potential candidates in the prevention and treatment of diseases via modulation of biological activities, Int. J. Phys. Pathophy. Pharma. 6 (2014) 125–136.
[36] P.R. Shirin Adel, J. Prakash, Chemical composition and antioxidant properties of ginger root (Zingiber officinale), J. Med. Plants Res. 4 (2010) 2674–2679.
[37] F. Tavakoli, M. Salavati-Niasari, F. Mohandes, Green synthesis and characterization of graphene nanosheets, Mater. Res. Bull. 63 (2015) 51–57.
[38] F. Tavakoli, M. Salavati-Niasari, F. Mohandes, Green synthesis of flower-like CuI microstructures composed of trigonal nanostructures using pomegranate juice, Mater. Lett. 100 (2013) 133–136.
[39] G. Yen, P. Duh, C. Tsai, Relationship between antioxidant activity and maturity of peanut hulls, J. Agric. Food Chem. 41 (1993) 67–70.
[40] P. Siddhuraju, P. Mohan, K. Becker, Studies on the antioxidant activity of Indian Laburnum (Cassia fistula L.): a preliminary assessment of crude extracts from stem bark, leaves, flowers and fruit pulp, Food Chem. 79 (2002) 61–67.
[41] N. Turkmen, F. Sari, Y. Velioglu, Effects of extraction solvents on concentration and antioxidant activity of black and black mate tea polyphenols determined by ferrous tartrate and Folin-Ciocalteu methods, Food Chem. 99 (2006) 835–841.
[42] X. Huang, J. Zhang, L. Wang, Q. Zhang, Simple and reproducible preparation of barium hexagonal ferrite by adsorbent combustion method, J. Alloys Compd. 540 (2012) 137–140.
[43] S.K. Chawla, R.K. Mudsainiyan, S.S. Meena, S.M. Yusuf, Sol–gel synthesis, structural and magnetic properties of nanoscale M-type barium hexaferrites BaCoxZrxFe(12−2x)O19, J. Magn. Magn Mater. 350 (2014) 23–29.
[44] M.K. Raju, FT-IR studies of Cu substituted Ni-Zn ferrites for structural and vibrational investigations, Chem. Sci. Trans. 4 (1) (2015) 137–142, 2015.
[45] I. Sadiq, I. Ali, E. Rebrov, S. Naseem, M.N. Ashiq, M.U. Rana, Nanosized Ce–Zn substituted microwave absorber material for X-band applications, J. Magn. Magn Mater. 370 (2014) 25–31.
[46] M.U. I Ali, M.S. Awan, M. Ahmad, M.A. Iqbal, Structural, electrical, and microstructure properties of nanostructured calcium doped Ba-hexaferrites synthesized by sol-gel method, J. Supercond. Nov. Magnetism 26 (2013) 3277–3286.
[47] M. Ahmad, R. Grössinger, M. Kriegisch, F. Kubel, M.U. Rana, Magnetic and microwave attenuation behavior of Al-substituted Co_2W hexaferrites synthesized by sol-gel autocombustion process, J. Curr. Appl. Phys. 12 (2012) 1413–1420.
[48] M.J. Iqbal, M.N. Ashiq, I.H. Gul, Physical, electrical and dielectric properties of Ca-substituted strontium hexaferrite ($SrFe_{12}O_{19}$) nanoparticles synthesized by co-precipitation method, J. Magn. Magn Mater. 322 (2010) 1720–1726.
[49] K.H.J. Buschow, F.R. de Boer, Physics of Magnetism and Magnetic Materials, Kluwer Academic Publishers, New York, Boston, Dordrecht, London, Moscow, 2004, pp. 75–83.
[50] B.X. Gu, Magnetic properties of $Ba_2Me_2Fe_{28}O_{46}$ (Me_2-X, Me=Ni, Cu, Mg, and Zn) hexaferrites, J. Appl. Phys. 70 (1991) 372–375.
[51] M. Tadic, D. Markovic, V. Spasojevic, V. Kusigerski, M. Remskar, J. Pirnat, Z. Jaglicic, Synthesis and magnetic properties of concentrated α-Fe_2O_3 nanoparticles in a silica matrix, J. Alloys Compd. 441 (2007) 291–296.
[52] A. Nadar, A.M. Banerjee, M.R. Pai, R.V. Pai, S.S. Meena, R. Tewari, A.K. Tripathi, Catalytic properties of dispersed iron oxides Fe_2O_3/MO_2 (M = Zr, Ce, Ti and Si) for sulfuric acid decomposition reaction: role of support, Int. J. Hydrogen Energy 43 (2018) 37–52.
[52a] A.R. Kagdi, N.P. Solanki, F.E. Carvalho, S.S. Meena, P. Bhatt, R.C. Pullar, R.B. Jotania, Influence of Mg Substitution on Structural, Magnetic and Dielectric Properties of X-type Barium-Zinc Hexaferrites Ba2Zn2-xMgxFe28O46, J. Alloys Compd. 741 (2018) 377–391.
[52b] C.C. Chauhan, A.R. Kagdi, R.B. Jotania, A. Upadhyay, C.S. Sandhu, S.E. Shirsath, S.S. Meena, Structural, magnetic and dielectric properties of Co-Zr substituted M-type calcium hexagonal ferrite nanoparticles in the presence of α-Fe2O3 phase, Ceram. Int. 44 (2018) 17812–17823, https://doi.org/10.1016/j.ceramint.2018.06.249.
[53] D. Ravinder, P.V. Bhaskar Reddy, P. Shalini, Frequency and composition dependence of dielectric behavior of copper substituted lithium ferrites, J. Mater. Sci. Lett. 22 (2003) 1599–1601.
[54] M.M. Haque, M. Huq, M.A. Hakim, Densification, magnetic and dielectric behaviour of Cu-substituted Mg-Zn ferrites, Mater. Chem. Phys. 112 (2008) 580–586.
[55] B.P. Rao, K.H. Rao, T. Vasantha, A. Paduraru, O.F. Caltun, DC resistivity and dielectric studies on Ti^{4+} substituted Ni-Zn ferrites, J. Optoelectron. Adv. Mater. 7 (2005) 701–704.
[56] C.G. Koops, On the dispersion of resistivity and dielectric constant of some semiconductors at audio frequencies, J. Phys. Rev. 83 (1951) 121–124.
[57] A. Aharoni, Introduction to the Theory of Ferromagnetism, Clarendon Press, Oxford, 1996.
[58] M.A. El Hiti, Dielectric behaviour in Mg-Zn ferrites, J. Magn. Magn Mater. 192 (1999) 305–313.
[59] J.C. Dyre, T.B. Schroder, Universality of ac conduction in disordered solids, Rev. Mod. Phys. 72 (2000) 873–892.
[60] S. Dutta, R.N.P. Choudhry, P.K. Sinha, Impedance spectroscopy studies on Ga-ion-modified PLZT ceramics, Phys. Status Solidi 202 (2005) 1172–1181.
[61] N. Pandsa, S. Pattanayak, H.B.K. Sharma, R.N.P. Choudhary, Structural and electrical properties of $BiFeO_3$–$PbTiO_3$ system, J. Mater. Sci. Mater. Electron. 26 (2015) 10012–10019.
[62] S.R. Ejaz, M.A. Khan, M.F. Warsi, M.N. Akhtar, A. Hussain, Study of structural transformation and hysteresis behavior of Mg-Sr substituted X-type hexaferrites, Ceram. Int. 44 (2018) 18903–18912.
[63] K.P. Padmasree, D.K. Kanchan, A.R. Kulkarni, Impedance and Modulus Studies of the Solid Electrolyte System 20CdI2-80 [xAg2O-Y(0.7V_2O_5-0.3B_2O_3)], where $1 \le x/y \le 3$, Solid State Ionics 177 (2006) 475–482.
[64] S.M. Patange, S.E. Shirsath, K.S. Lohar, S.S. Jadhav, N. Kulkarni, K.M. Jadhav, Electrical and switching properties of $NiAl_xFe_{2-x}O_4$ ferrites synthesized by chemical method, Phys. B Condens. Matter 406 (2011) 663–668.
[65] R.N. Bhowmik, I.P. Muthuselvam, Dielectric properties of magnetic grains in $CoFe_{1.95}Ho_{0.05}O_4$ spinel ferrite, J. Magn. Magn Mater. 335 (2013) 64–74.
[66] Y. Bai, J. Zhou, Z. Gui, L. Li, Electrical properties of non-stoichiometric Y- type hexagonal ferrite, J. Magn. Magn Mater. 278 (2004) 208–213.
[67] S. Narayanan, A.K. Baral, V. Thangadurai, Dielectric characteristics of fast Li ion conducting garnet-type $Li_{5+2x}La_3Nb_{2-x}Y_xO_{12}$ (x = 0.25, 0.5 and 0.75), Phys. Chem. Chem. Phys. 18 (2016) 15418–15426.